Self-organization process in newborn skin organoid formation inspires novel strategy for hair regeneration of adult cells

Mingxing Lei[a,b,c], Linus J. Schumacher[d,e], Yung-Chi Lai[c], Wen-Tau Juan[c,f], Chao-Yuan Yeh[a], Ping Wu[a], Ting-Xin Jiang[a], Ruth E. Baker[d], Randall Bruce Widelitz[a], Li Yang[b,1], Cheng-Ming Chuong[a,c,1]

[a]Department of Pathology, Keck School of Medicine, University of Southern California, 2011 Zonal Avenue, Los Angeles, CA 90033, USA.

[b]"111" Project Laboratory of Biomechanics and Tissue Repair & Key Laboratory of Biorheological Science and Technology of Ministry of Education, College of Bioengineering, Chongqing University, 174 Shazhengjie, Shapingba, Chongqing 400044, China.

[c]Integrative Stem Cell Center, China Medical University Hospital, China Medical University, 2 Yude Road, North District, Taichung 40402, Taiwan

[d]Mathematical Institute, University of Oxford, Woodstock Road, Oxford, OX2 6GG, UK.

[e]Department of Life Sciences, Imperial College, London, SW7 2AZ, UK

[f]Institute of Physics, Academia Sinica, 128 Academia Road, Section 2, Nankang, Taipei 11529, Taiwan

[1]Correspondence: Cheng-Ming Chuong, cmchuong@usc.edu; Li Yang, yanglibme@cqu.edu.cn

Short title: Self-organization in reconstituting hairy skin

Keywords hair neogenesis | stem cells | phase transition | environmental reprogramming | tissue engineering | wound healing

Abstract

Organoids made from dissociated progenitor cells undergo tissue-like organization. This *in vitro* self-organization process is not identical to embryonic organ formation, yet it achieves a similar phenotype as *in vivo*. This implies genetic codes do not specify morphology directly; instead, complex tissue architectures may be achieved through several intermediate layers of crosstalk between genetic information and biophysical processes. Here we use newborn and adult skin organoids for analyses. Dissociated cells from newborn mouse skin form hair primordia bearing organoids that grow hairs robustly *in vivo* after transplantation to nude mice. Detailed time-lapse imaging of three-dimensional cultures revealed unexpected morphological transitions between six distinct phases: dissociated cells – cell aggregates – polarized cysts – cyst coalescence – planar skin – hair-bearing skin. Transcriptome profiling reveals the sequential expression of adhesion molecules, growth factors, Wnts, and MMPs. Functional perturbations at different times discern their roles in regulating the switch from one phase to another. In contrast, adult cells form small aggregates but then development stalls *in vitro*. Comparative transcriptome analyses suggest suppressing epidermal differentiation in adult cells is critical. These results inspire a new strategy that can restore morphological transitions and rescue the hair-forming ability of adult organoids: 1) continuous PKC inhibition; and 2) timely supply of growth factors (IGF, VEGF), Wnts, and MMPs. This comprehensive study demonstrates alternating molecular events and physical processes are in action during organoid morphogenesis, and that the self-organizing processes can be restored via environmental reprogramming. This tissue-level phase transition could drive self-organization behavior in organoid morphogeneis beyond the skin.

Significance

This study opens new avenues to improve the ability of adult skin cells to form a fully functional skin, with clinical applications. Our investigation elucidates a relay of molecular events and biophysical processes at the core of the self-organization process during tissue morphogenesis. Molecules key to the multi-stage morphological transition are identified and can be added or inhibited to restore the stalled process in adult cells. The principles uncovered here are likely to function in other organ systems and will inspire us to view organoid morphogenesis, embryogenesis, and regeneration differently. The application of these findings will enable rescue of robust hair formation in adult skin cells, thus eventually helping patients in the context of regenerative medicine.

\body

Introduction

Recent studies have made substantial progress in three-dimensional (3D) organoid cultures. Multiple epithelial organoids have been generated that resemble their counterparts *in vivo,* such as the mammary gland (1, 2), salivary gland (3), stomach, colon, pancreas ducts, and liver bile ducts (4). Using stem cell biology approaches, scientists have also generated the cerebral cortex (5) and optical cup (6). The common feature of these organoids is that they are generated by 3D culture of isolated tissue progenitors or pluripotent stem cells, and that a proper environmental context is provided to guide cells to differentiate into multiple cells types with proper tissue organization. These cultures start from dissociated cells that have lost external cues and, amazingly, they can still reform organized tissues similar to those produced during embryonic development *in vivo*, albeit with different degrees of tissue organization compared to the normal organ morphology.

Organoid cultures have been used as a disease model, and can provide organized tissues for regenerative medicine (7). Yet, organoid formation also provides a new and unique opportunity which is not fully developed: to decipher fundamental principles of the self-organization processes (8). Self-organization is the spontaneous formation of ordered structures from a group of progenitor cells that have no ordered pre-pattern. This can be viewed as a developmental biology question: how do

embryonic cells organize in different ways to generate diverse organs and body forms (9)? It is clear that we do not fully understand how one-dimensional DNA codes generate three-dimensionally organized topologies (10). The genetic codes do not encode morphology directly, instead complex tissue architectures are achieved through several intermediate layers of interactions involving physical and genetic mechanisms (11, 12). Yet, how such genetic information and physical processes crosstalk and intertwine with one another to achieve morphological phenotypes remains to be elucidated. However, this knowledge has significant implications for improving our ability to deliver more complex organoids.

The skin organ is a consummate model for studying self-organization processes because of its accessibility to experimentation, its relatively flat configuration and the availability of genetic tools in mice (13-15). Previous studies have shown that a mixture of dissociated newborn mouse epidermal and dermal cells can reconstitute and form *de novo* hair follicles *in vivo* (16-19). These grafts formed a reconstituted organized skin with orientated hair follicles that undergo cyclic renewal and can respond to injury and regenerate (19). However, the principles underlying self-organization behavior by stem cell collectives remain elusive. Moreover, although the skin cells derived from newborn mice and adult mice share the same genome, adult cells lose this regenerative ability (20). Thus, it has been difficult to generate organized tissues derived from adult cells. Skin reconstituted from human cells does form hairs, but not as robustly as that reconstituted from cells derived from newborn mice (21-23). Thus, there is a great need to learn more about the fundamental conditions required by skin cells to regenerate a functional skin, and to identify key environmental factors which will facilitate the hair forming ability in more easily obtained adult mouse cells, and eventually human cells.

In the present study, we developed a two-step method to produce hair-bearing skin: we elucidated *in vitro* culture conditions that enable skin organoids to form from dissociated cells; and transplant techniques that allow organoid explants to form skin with hairs that show normal hair architecture (24). The *in vitro* step provides two major advantages. First, it allows time-lapse analysis of cell behaviors occurring within the 3D droplet, i.e. 4D analyses of the dynamic temporal changes in

tissue morpho-space. To our surprise, cells undergo a series of unexpected complex morphological transitional processes to go from dissociated cells into a planar layer of presumptive skin. These findings led us to develop the idea that a series of phase transition-like processes takes place at the level of the cell population, and that these phase transitions could constitute one of the major physical processes used in tissue self-organization. The second advantage to *in vitro* culture is that it allows experimental manipulation of the molecular mechanisms involved. Transcriptome profiling reveals four stages of molecular expression, and allows us to identify molecules that enhance or suppress morphological transitions between each stage. To validate our hypotheses for tissue self-organization, we employ dissociated cells generated from adult skin, which normally does not form hairs, and are able to restore the hair-forming ability of adult mouse cells.

Our results offer new promise to improve the ability of human skin cells to form more hair follicles in a fully functional skin, which has clear clinical applications. For basic science, this work demonstrates that a relay of molecular events and physical processes may be core to the self-organization process during tissue morphogenesis. In this case, morphogenetic behavior analyses prompted us to borrow the biophysical concepts of coagulation and self-assembly to explain the morphological phase transitions observed. It seems genes do not encode morphology directly. Instead, complex tissue patterns are achieved through several intermediate layers of interactions involving “physico-genetic” mechanisms (11, 12). This concept can be applied to understand self-organizing process in organoid morphogenesis beyond the skin and is discussed further.

Results

Dissociated Progenitor Cells Form Planar Skin *in vitro* Via a Stepwise, Self-organizing Process

Neonatal mouse dorsal skin is separated into epidermis and dermis. Each tissue is then dissociated into single cells (Fig. 1*A*). A mixture of epidermal and dermal cells is grown as 3D cultures on cell culture inserts in a transwell system, forming an air-liquid interface (SI Appendix, Fig. S1*A*). Phase-contrast microscopy shows white patches were formed at day 1 (SI Appendix, Fig. S1*B*).

Immunostaining for K14 and K10 indicates those patches originate from basal epidermal cells rather than suprabasal epidermal cells (SI Appendix, Fig. S1*B*-*C*).

Interestingly, immunostaining and H&E staining showed these epidermal aggregates display morphological changes during culture (Fig. 1*B*-*C* and SI Appendix, Fig. S1*D*-*E*), which reveal a self-organization process through six consecutive stages. Stage 0, *Dissociated cells*. Stage 1, *Aggregates*. Unequal sized aggregates form at day 1. Stage 2, *Cysts*. More equally sized polarized aggregates containing ~350 cells form at day 2, surrounded by 2-3 dermal cell layers forming skin spheroids. The polarized aggregates become cystic at day 3, filled with keratin, here stained by eosin. Stage 3, *Coalesced cysts.* Epidermal cell bridges link the cysts which fuse to form epidermal planes, around day 4 - 5. Stage 4, *Planar skin*. The small epidermal planes further merge to form a large plane from day 5.5 - 7. Notably, at about day 5.5 - 6, the large plane forms a bilaterally symmetric double layered epidermal structure, with each layer covered by dermal layers facing the liquid or air phase, respectively. The large epidermal planes further coalesce and descend to the bottom of the culture insert at the liquid phase, forming stratified layers from day 6 to 10. The epidermal and dermal planes are clearly distinguished by epidermal and dermal markers, respectively (SI Appendix, Fig. S1*F-G*). Stage 5, *Hair placode induction*. At day 10 to 11, hair-placode-like structures are induced (SI Appendix, Fig. S1*H*). Robust hair follicles with normal structures are regenerated when this explant is transplanted to the back of nude mice, and the regenerated hair follicles are derived from donor cells (Fig. 1*D*). Interestingly, when we culture the cells at a submerged condition, the epidermal cells can also self-organize as those in air-liquid culture condition. The epidermal plane is also formed at the culture insert side (SI Appendix, Fig. S1*I*).

The ratio of epidermal: dermal (E:D) cells influences epidermal cell aggregation (SI Appendix, Fig. S2*A*). Compared with aggregate formation using combinations of epidermal and dermal cells (1:9 ratio), very small aggregates form when only epidermal cells are cultured, indicating the self-organization process is dermal cell-dependent. We assumed that a higher E:D ratio would lead to larger aggregate formation. Unexpectedly, a higher E:D ratio causes smaller aggregates to form and

vice versa. We next sought to isolate pure epidermal and dermal populations using FACS sorting. 3D mixed cultures of pure populations from FACS-sorted K14-GFP+ epidermal and Pdgfra-EGFP+ dermal cells at a ratio of 1:9 produced similar sized aggregates (SI Appendix, Fig. S2*B*-*C*).

Adult cells fail to self-organize

When adult mouse cells are used in a parallel mixed cell reconstitution assay, epidermal cells only form a few small aggregates which do not grow, as demonstrated by immunostaining for specific markers (Fig. 1*E*-*F* and SI Appendix, Fig. S2*D*). Lowering E:D cell ratio to 1:30 produces larger aggregates which undergo terminal differentiation and fail to coalesce at day 4 (SI Appendix, Fig. S2*E*). Transplanting those adult cells at different E:D ratios to the dorsum of nude mice produced very few hairs compared to the robust hair follicle regeneration seen with newborn mouse cells (Fig. 1*D* and SI Appendix, Fig. *S2E*). These assays demonstrate that cells from newborn mice have a greater capacity for self-organization and tissue regeneration in this assay than cells derived from older mice (>2-month-old), and the self-organization capacity of cells is required for prospective tissue regeneration.

To further confirm dermal cells are required for epidermal cell self-organization, we did recombination assay, including newborn epidermal cells + adult dermal cells (NE+AD) and newborn dermal cells + adult epidermal cells (ND+AE). The result shows that ND+AE group undergo more similar self-organization process to the newborn mouse cells (SI Appendix, Fig. S2*F*). The epidermal cells form small aggregates at day 1, which grow larger and form cysts at day 3. Partial cysts undergo coalescence at day 4 and form a double-layered epidermal plane at day 7. However, the epidermal cells from NE+AD group form very small aggregates at day 1, which cannot further polarize at day 3 or coalesce at day 4, resulting in terminal differentiation at day 7. Transplanting those cells onto the nude mice form very few hairs, when compared to the ND+AE group, which form a lot of hairs.

Live imaging of cellular behaviors during organoid formation

To observe how cells behave in this assay, we set up a time-lapse live imaging system using fluorescent confocal microscopy to visualize and quantify cell motility (SI Appendix, Fig. S3*A*). Five major stages of cellular behaviors were observed before hair placode induction based on live-imaging of K14-GFP mouse (25) cells showing the epidermal basal component (Movie S1).

1) *Dissociated cells.* Cells are dissociated at the very beginning.

2) *Aggregation*. During random epidermal cell movement from 0 h to 3 h (Movie S1) two or more cells will collide. These cellular contacts lead to the formation of aggregates at two days that progressively increase in size. Interesting observations were made during epidermal cell aggregation: a. *Modes of aggregate formation*. Large aggregates form through the random addition of single cells, or by merging two or more small aggregates, or by a combination of these two mechanisms (Fig. 2*A* and SI Appendix, Fig. S3*B*). b. *Shape of aggregates*. Aggregates form as round balls with a coarse surface. c. *Unstable fusion of aggregates*. At 7 – 12 h cells form aggregates (Fig. 2*A*) but a few aggregates are unstable. Live imaging shows cells/small aggregates can join an aggregate and then leave (Fig. 2*A*, purple arrow and SI Appendix, Fig. S3*C*-*E*), albeit aggregation is far more frequent than dissociation, so that overall aggregates form and grow. Small aggregates also can merge to form larger aggregates (Fig. 2*B*). Big aggregates can, but rarely, disaggregate into smaller components (Fig. 2*C*).

Cell tracking revealed that epidermal cells move in an undirected manner, i.e. with low directional persistence, throughout the experiment (Fig. 2*E*). Furthermore, cell velocities decrease as more cells are in clusters. Thus we were motivated to describe epidermal cell aggregation, as a first approximation, using the Smoluchowski coagulation equations (Smoluchowski, 1916) with a size-dependent aggregation rate (SI Appendix, Fig. S3*F)*. Numerical solutions to these equations match aggregate cluster size-distributions from the initial stage of the aggregation process (Fig. 2*F*). The only free parameter in this model is the overall aggregation rate constant. In addition to fitting the numerical solution to the data, we collapse the size-distributions from different time-points onto a single curve (SI Appendix, Fig. S3*G*) by rescaling relative to the average cluster size at each time-

point, confirming the aggregation model in a parameter-free manner. Size-distributions from the 48-hour time-point do not scale as predicted by the theory (SI Appendix, Fig. S3*G*), indicating a change in cluster growth dynamics during the transition to stage 2, when aggregates develop polarity and interact with dermal cells through the formation of a basement membrane.

3) *Polarization*. Cell aggregates stop growing when the outer epidermal cells become crescent-shaped, suggesting the polarization of aggregates and the conversion of cell aggregates into cysts (Fig. 2*B*-*C*). At this time, the epidermal cysts are encircled with 2-3 layers of dermal cells that show dynamic and random movements (Fig. 2*D* and Movie S2*A*).

4) *Coalescence*. With increasing time, more and more cells undergo apoptosis in the center of the aggregate, forming a cyst; while some outer cells still dynamically circle around the aggregate (Fig. 2*G*). The cystic aggregates start a dynamic merging process at about day 4 which can occur through two means 1) nearby aggregates can directly merge together (SI Appendix, Fig. S3*H* and Movie S2*B*); and 2) a group of epidermal cells protrudes from more distant aggregates, leading to the coalescence of cysts (Fig. 2*H*).

5) *Planar skin formation*. The merged cysts continue to coalesce to form an even larger plane, through the protrusion of an epidermal chain or by adjacent fusion of smaller planes (Fig. 2*I*). Then the lower epidermal plane becomes differentiated at day 7. From day 9 to day 10, the epidermal cells become relatively quiescent again (Movie S1).

We also examined dermal cell behavior by observing Pdgfra-EGFP mouse cells (Movie S3), which represents all dermal cell lineages (26). Six major stages were observed comparable to the epidermal cells (Fig. 2*J*). 1) *Dissociated cells* (0 hr). 2) *Random movement* and initial association with epidermal cells. At 8h, most of the dermal cells remain dissociated and move quickly and randomly. A few cells become associated with the dark region representing the epidermal aggregate. 3) *Encirclement* of dermal cells around the epidermal cyst. A subpopulation of dermal cells forms single to multiple layers of concentric circles surrounding the epidermal cells from day 1 to day 4. This was also visualized by using a FVB-GFP mouse in which all the cells fluoresce (Movie S2*A*). 4)

Reorganization. As the epidermal cysts merge, the dermal cells move away from the inter-aggregate region (Movie S2 and S3*B*). The dermal cells then gradually move up above the epidermal cells to the air phase from day 4 to day 10. 5) *Dermal plane formation*. The dermal cells gradually cover all the epidermal cells, and form the dermal plane. By using a K14-GFP/Lef1-RFP transgenic mouse, we show that Lef1+ papillary dermal cells are located adjacent to K14 positive epidermal cells (Movie S2*C*). The dermal cells become more quiescent when the dermal plane forms at day 7, and is maintained through day 10. 6) *Dermal condensation*. Some dermal condensates are observed at Day 11-12 (Movies S2*C* and S3).

Transcriptome profiling during the self-organization process to form skin

To explore the molecular basis of the self-organization process, we performed RNA-sequencing (RNA-seq) in duplicate at seven time points (SI Appendix, Fig. S4*A*), showing six groups of genes that were differentially expressed at different stages (Fig. 3*A,* SI Appendix, Fig. S4*A*-*C* and Table S1). Those genes were further classified into four major categories based on cellular processes (Fig. 3*B*).

1. *Aggregation*. Known principles of organ self-assembly are based on the sorting of cells with similar adhesive properties, where differential cell fate decisions are due to distinct spatial distributions (7, 8). Indeed, in our system, RNA-seq data show adhesion molecules such as Cdh1 were highly expressed at the initial stage at 6h (Fig. 3*B* and SI Appendix, Fig. S4*D*). Besides, gene ontology shows genes involved in the insulin signaling pathway (e.g. *Prkaa1*, *Pik3ca*) and NOD-like receptor signaling pathways (e.g. *Pdgfb*) are also increased at 6h (Fig. 3*A*-*C* and SI Appendix, Fig. S4*D*). At day 1, many collagen genes are increased (e. g. *Col1a1*, *Col4a1*) and another group of cell adhesion and focal adhesion genes (e.g. *Pik3r1*) are up-regulated (SI Appendix, Fig. S4*C*-*D*).

2. *Polarization*. At 48h, the polarized aggregate stage, several genes involved in the IGF (e.g. *Igfbp3*) and Vegf (e.g. *Vegfc*, *Prkcb*) signaling pathway are up-regulated. Additional extracellular matrix (e.g. Col4a1) genes are increased at day 2 (Fig. 3*B*-*C* and SI Appendix, Fig. S4*D*). Genes involved in basement membrane formation and cell-cell junctions are also enhanced.

3. *Coalescence*. At day 4, some extracellular matrix molecules including Wnt (e. g. *Wnt10a*) family members are increased (Fig. 3*A*-*C* and SI Appendix, Fig. S4*D*). Wnts are reported to induce MMP expression (27, 28). Indeed, we observed a group of MMP genes (e.g. *Mmp13*, *Mmp14*) are expressed at this time point (Fig. 3*A*-*C* and SI Appendix, Fig. S4*D*). In contrast, collagen genes including *Col1a1* and *Col4a1* and those involved in TGF signaling (e.g. *Tgfb3*) are down-regulated (Fig. 3*B*-*C* and SI Appendix, Fig. S4*D*). The cellular behavior of epidermal cell coalescence resembles cancer cell invasion. Interestingly, gene ontology shows pathways involved in cancer are significantly increased at this stage (Fig. 3*A*).

4. *Planar skin formation*. When planar skin was formed from day 6 to day 10, we found many genes (e.g. *Nfkb2*) involved in Toll-like receptor signaling are up-regulated, and genes related to NF-kB signaling and lysosome mediated apoptosis (e.g. *Ctsl* family) are increased (Fig. 3*A*-*C* and SI Appendix, Fig. S4*C*-*D*). At day 10, another group of epidermal differentiation complex (EDC) genes carrying precursors for cornified envelope such as the *Sprr* gene family members, are increased (SI Appendix, Fig. S4*C*-*D*).

5. *Hair primordia*. Hair follicle development related genes such as multiple Wnt genes (e.g *Ctnnb1*, *Wnt3a* and *Wnt5a*) are increased, which might initiate periodic patterning (SI Appendix, Fig. S4*C*-*D*). Hair follicle morphogenesis was largely investigated in previous studies (29), thus we focused on the earlier stages in the present study.

Spatiotemporal genes expression during the self-organization process

To investigate the spatiotemporal expression of genes identified by RNA-seq, we performed immunostaining and in situ hybridization. We chose the specific genes and pathways based on the following three principles: 1) The functional annotation of the selected pathway should have significance with the p-value ($p < 0.05$); 2) The genes in those pathways selected to do immunostaining or in situ hybridization should be at a detectable level. For this, we checked the gene expression by looking their RPKM (Reads Per Kilobases per Million reads) value (usually larger than

25 for gene expression study). 3) The phenotypes observed in the morphological transition processes were also matched with functional annotations, to target the potential genes or pathways in these top enriched pathways.

We observed adhesion molecules including β-catenin, NCAM, P-cadherin (*Cdh3*) and E-cadherin (*Cdh1*) are strongly expressed in the epidermal cells, particularly at the border of the cyst (Fig. 4*A* and SI Appendix, Fig. S5*A*-*B*). We also selected one sample gene representing each highly enriched signaling pathway to test by *in situ* hybridization. The results show that *Igfbp3*, *Vegfa* and *Tgfbi* are expressed in the dermis surrounding the epidermal aggregates (SI Appendix, Fig. S5*C*). A basement membrane forms at the outer part of the cyst, shown by Collagen type I and type IV, and Lamc2 expression (Fig. 4*B* and SI Appendix, Fig. S5*D*). Many cells undergo apoptosis and stop proliferating in the center of the cyst after day 2 (SI Appendix, Fig. S5*D*).

At day 4, during epidermal aggregate coalescence, the chain of cells that protrudes from the aggregates expresses E-cadherin, P-cadherin, β-catenin, Dsc3 and Dsg3 (SI Appendix, Fig. S5*E*), indicating its epidermal identity. MMPs may play a role in breaking the basement membrane to release the epidermal cells from the aggregate. We tested *Mmp14* and *Mmp13* expression, which were highly up-regulated based on our RNA-seq analysis. *Mmp14* is observed both in the basal layer of the aggregate and the dermal cells surrounding the aggregate at day 3.5. Also, *Mmp14* expression was occasionally observed in the dermal chain (Fig. 4*C*). *Mmp13* is preferentially expressed at the liquid phase of the aggregates from day 3.5 (SI Appendix, Fig. S5*F*).

The inner part of the cyst also fused together after the cyst coalesces. In situ hybridization shows genes involved in epidermal differentiation are expressed in this same region which becomes the suprabasal layer of the planar skin (Fig. 4*D* and SI Appendix, Fig. S5*G*).

In summary, the spatiotemporal expression of molecules in both epidermal and dermal cells may trigger epidermal and dermal interactions in different phases. For example, the dermal microenvironment secretes extracellular matrix (ECM) including collagens that facilitate basement membrane formation at day 2, then is broken by the MMPs at day 4, which may lead to the dynamic

cellular behaviors observed between stage 1 and stage 4 during the self-organizing planar skin forming process (SI Appendix, Fig. S5*H*). Our findings suggest that different classes of molecules are required to transition between different stages of skin organoid morphogenesis. It should be noted these are early events that precede periodic formation of hair primordia.

Molecular perturbation of the skin organoid formation process

From dissociated cells to cellular aggregates. To determine the possible involvement of the differentially expressed genes in regulating the switch of morphological phases, we carried out functional perturbation by applying small molecule inhibitors or recombinant proteins highlighted by RNA transcriptome analyses in the cultures at different time points.

Small aggregates formed from epidermal cells alone without dermal cells (SI Appendix, Fig. S2*D*), yet they failed to grow larger, indicating that dermal signals are required for further epidermal cell aggregation. *Pdgfb*, which is secreted by dermal fibroblasts, started to be increased at 6h. The aggregate size was significantly increased at day 1 and day 2 when inhibitors of *Pdgfb*, or *Pdgf* receptors were applied at 0h (Fig. 5*A*-*B* and Fig. S6*A*-*B*). *Pik3cg*, involved in the IGF pathway, was reported to be an important modulator of extracellular signals, including those elicited by E-cadherin-mediated cell-cell adhesion (30). Inhibiting PI3K function with Ly 294002 resulted in larger aggregate formation (SI Appendix, Fig. S6*A*-*B*). Conversely, the aggregate size was significantly decreased when IGF (e.g. *Igf2*, and *Igf1r*) and VEGF (e.g. *Vegf2* and *Vegfrs*) family members were inhibited (Fig. 5*A*-*B*, SI Appendix, Fig. S6*A*-*B* and Movie S4 for IGF inhibition).

***From cell aggregates to coupled epidermal – dermal cysts*.** The apical-basal polarity of aggregates formed at day 2. To test whether collagens are involved in this process, we added recombinant Collagen I or IV proteins to the cells. These proteins homed to the dermal cell region and displayed longer fibers at day 1 (SI Appendix, Fig. S6*C*). The results reveal Collagen I and IV have at least two functions during epidermal aggregation. Live-imaging showed formation of a long epidermal cell strand with some epidermal cells migrating along the strand when recombinant Collagen I protein

was added to the cells at day 1 (SI Appendix, Fig. S5*D* and Movie S5*A*), indicating collagen fibers may facilitate epidermal cell movement and bridge aggregates which then merge together. Later, cells treated with recombinant Collagen I or IV protein formed more concentric aggregate layers at day 2 and day 3 (Fig. 5*C*, SI Appendix, Fig. S6*E* and Movie S5*B*), suggesting those collagens promote aggregate assembly. P-cadherin immunostaining showed that aggregate A-P polarity formation was accelerated after Collagen types I and IV protein treatment (Fig. 5*C*-*D* and SI Appendix, Fig. S6*E*), with very smooth border formation at day 1, compared to the coarse border found in control samples. Interestingly, aggregates with smooth borders formed at day 1 when inhibitors of TGFβ-RI, PKR and Class III tyrosine kinase are added at 0h (SI Appendix, Fig. S6*F* and Movie S6*A* for TGFβ-RI). Atypical PKC was reported to be involved in epidermis polarity formation (31). After inhibiting PKC activity with Bisindolylmaleimide, P-cadherin immunostaining reveals that aggregate size is unaffected but polarity is lost (Fig. 5*C*-*D*).

***Coalescence of cysts*.** During the coalescence stage (around day 4), a group of epidermal cells protrudes out from the aggregates. This process can be accelerated by inhibiting EGF signals, or activating Wnt signaling (Fig. 5*E*-*F* and SI Appendix, Fig. S7*A*-*B*). When inhibitors or agonists targeting these pathways were added to the culture at day 1, 70% of aggregates coalesced by day 3, compared to ~15% for controls (Fig. 5*E*-*F* and SI Appendix, Fig. S7*A*-*B*).

We next pursued how the polarized aggregates coalesce. The basement membrane of the aggregate needs to break to release epidermal cells. We speculated that MMPs play a role in this process. Indeed, when the MMP inhibitor Prinomastat was added to the cultures, live-imaging of K14-GFP epidermal cells showed blocked aggregate coalescence at day 3.5 (Fig. 5*E*-*F* and Movie S7*A*-*C*). This also was evidenced by imaging cellular behaviors of Pdgfra-EGFP labeled dermal cells, which show dermal cell movement and blocking of epidermal aggregate coalescence (SI Appendix, Fig. S7*C* and Movie S7*D*-*E*).

***Lamella formation*.** The cysts descend to the bottom of the culture insert at day 6. We wondered whether the differential expression pattern of *Mmp13* (SI Appendix, Fig. S5*F*) might be involved in this

process. When the selective potent MMP13 inhibitor, Way 170523, was added, the aggregates showed less coalescence and failed to descend down to the liquid phase (Fig. 5*G*-*H*). From RNA-seq data, we observed increased *Nfkb2* and *Ctsl* expression at the coalescence stage. K14 immunostaining reveals that specific inhibitor-mediated protein inactivation facilitates cyst coalescence and promotes sinking down of cysts (Fig. 5*G*-*H* and SI Appendix, Fig. S7*D*). In addition to influencing smooth border formation of the aggregates (Movie S9A), Laminin, which is normally highly expressed at day 4 is required to promote further coalescence of the small epidermal plane to form a large epidermal plane. Inhibition of laminin blocked this further coalescence process (SI Appendix, Fig. S7*D* and Movie S8*B*). Together, the positive and negative molecular modules at different time points direct progression of self-organization during skin organoid formation (Fig. 5*I*).

Dermal cells used for periodic patterning are from papillary dermis

In addition to epidermal cell patterning, we also examined which dermal cell population enhanced planar skin formation in culture. *Lrig1* and *Dlk1* are expressed in the upper and lower dermis, respectively, during skin development. Those different populations have different hair follicle regenerative abilities during reconstitution (32). In the present study, RNA-seq data showed that *Dlk1* expression was quickly lost at day 1 and *Lrig1* was decreased but maintained at a certain level during culture, indicating that the dermal cells of the reconstituted skin originated from the upper dermis (SI Appendix, Fig. S6*E*). Using a K14-GFP/Lef1-RFP mouse in the reconstitution assay, we observed Lef1-RFP positive cells that belong to the papillary dermis were located adjacent to the epidermal plane (SI Appendix, Fig. S7*F* upper panel and Movie S3*C*). This is also indicated by Lef1 immunostaining, which shows that 3-4 layers of Lef1-positive cells are located beside the epidermal plane (SI Appendix, Fig. S7*F* lower panel). These dermal cells can form dermal condensate-like structures that are alkaline phosphatase positive (SI Appendix, Fig. S7*G*). The dermal condensate was also observed by culturing skin cells from a Sox2-EGFP transgenic mouse at day 11 (SI Appendix, Fig. S7*G*). Transplanting these cultures into nude mice results in formation of hair follicles

with irregular spacing between each hair follicle, when compared to the even-spaced buds between hair follicles that are physiologically developed during embryogenesis in mouse (SI Appendix, Fig. S7H). This suggests the reconstituted skin is competent to form new placodes, but the competence in different parts of the explants may not achieve at the same time, giving rise to the irregular pattern observed here. More studies will be needed to investigate this phenomenon further.

Rescuing the hair regeneration ability of adult mouse skin cells by restoring the self-organization process

We further tested whether the principles governing morphological transitions in newborn mouse cells could be applied to restore the self-organizing abilities of adult mouse cells (>2-month-old) to form hair-bearing skin. We performed RNA-seq using adult cell derived organoid cultures and compared the results with those using newborn cells at corresponding time points (SI Appendix, Fig. S8A-D). Both newborn and adult cells can form small aggregates but adult cell aggregates stall before the aggregates grow larger (Fig. 1*E*-*G*). As such, we selected genes that are up-regulated in both newborn cells and adult cells at 6h that foster cell aggregation, and genes up-regulated in only newborn cells but not in adult cells at day 1 and day 2 that may be responsible for later phase transition-like events (Fig. 6*A* and SI Appendix, Fig. S8*C*-*D*).

The gene ontology results show that genes involved in the *Igf* and *Vegf* signaling pathways are highly enriched in both newborn and adult cells at 6h, but upregulated in newborn cells when compared to adult cells at day 1 and day 2 (SI Appendix, Fig. S8*E*). Some Wnt genes such *Rspo2*, *Wnt3a* and *Wnt10b* are also expressed at a higher level in newborn cells (Fig. 7*A*). The biggest difference we observed is that adult cells quickly differentiate in culture. Compared to the newborn culture in which epidermal differentiation genes become enriched at later stages (D7), many EDC genes start to be enriched from 6h or day 1 in adult cultures (Fig. 6*B* and SI Appendix, Fig. S8*F*), which could be one of the main reasons that cells lose their competence to regenerate hairs and terminally differentiate.

Based on transcriptome analyses and functional studies, we have found that altering the expression of just one molecule at a time does not produce impressive advances in restoring hair formation. Here, guided by our new concept learned from newborn skin cultures, we are able to design a systemic pathway to restore the organoid formation process. We set up a stepwise method to re-induce the self-organization process per our RNA-seq analyses (Fig. 6*C*). We first added multiple growth factors including IGF and VEGF at the initial stage. We then added Wnt3a or Wnt10b recombinant proteins at day 1, due to their dual function in newborn cells, including enlarging aggregate size and accelerating aggregate coalescence, and due to their reduced expression in adult cells. Also, we added MMPs from day 3 to trigger the coalescence of aggregates. Importantly, to prevent epidermal cell differentiation, we added PKC inhibitors throughout the whole cultivation period.

The results show that addition of IGF2, IGFBP3 or VEGF2 recombinant proteins lead to an enlarged aggregate size (Fig. 6*D*-*E* and SI Appendix, Fig. S8*G*-*I*). Strikingly, a single addition of IGF2, IGFBP3 or VEGF2 recombinant proteins is sufficient to induce aggregates to significantly enlarge in size at day 1 and day 2, but they then terminally differentiate at day 3 (SI Appendix, Fig. S8*G*), indicating those factors can enhance cell adhesion but cannot maintain their planar skin forming properties. Addition of Wnt3a or Wnt10b recombinant proteins at day 1 further increases aggregate size at day 2 and induces epidermal cell chain protrusions at day 3. In fact, a single addition of Wnt3a or Wnt10b at time 0 is also sufficient to enlarge aggregate size at day 2, although with a lower density of hair regeneration probability upon transplantation (SI Appendix, Fig. S8*J*-*K*). Coalescence of aggregates occurred when MMP14 recombinant protein was subsequently added. These coalesced aggregates can directly descend to the liquid phase and form symmetric epidermal layers, indicating that signals involved in aggregate descent are induced. These “restored” adult organoids were then transplanted to the dorsum of nude mice, where regeneration of hair follicles increased from 0% to around 40% of the levels seen with newborn cell organoid cultures (Fig. 6*D*, *F* and SI Appendix, Fig.

S8*H*, n=9). K14-GFP shows the regenerated hair follicles are derived from donor cells (SI Appendix, Fig. S8*L*).

DISCUSSION

The self-organizing process of planar skin formation from dissociated cells is counter-intuitive

We have developed a 3D *in vitro* organoid model, in which dissociated newborn mouse skin cells are cultured at high density. This gives us the unique opportunity to visualize the process leading from individual cells to skin with time-lapse movies. Within a 10-day period, we observed that the dissociated cells progress through a series of morphological phase transitions to achieve a planar layer of presumptive skin with hair primordia (Fig. 7). Grafting of this explant to nude mice with a full thickness skin wound leads to well-formed reconstituted skin with robust hair growth. These hair follicles have normal architecture and can undergo cyclic regeneration, fulfilling the definition of tissue engineered hair follicles (33, 34).

However, close inspection of this process revealed two surprises. First, in skin development, presumptive skin covers the body surface, then periodically arranged dermal condensation and epidermal placode start to emerge around embryonic day 14. *In vitro,* it is remarkable because the dissociated cells, having lost all external cues in developing embryos, can reroute and traverse a different morphogenetic path to acquire the same phenotype as they do *in vivo*. This is not what one would expect if morphogenesis were to occur based on a simple molecular blueprint. Instead, it indicates that more fundamental self-organization principles are followed by the dissociated cells to achieve their final morphology.

Second, planar skin has a simple configuration consisting of an epidermis and a dermis, with a basement membrane in between. Thus, one may intuitively consider that dissociated epidermal and dermal cells, mixed in suspension, could simply sort themselves out and form sandwich-like cellular layers. Instead, the cells in our assay take a tortuous route from dissociated cells to aggregate →

polarized cysts → coalescing cysts → planar hair-bearing skin. We postulate that direct formation of the final, layered skin may well violate physical constraints imposed by the nature of the active material that the mixture of cells constitutes. Instead, the morphological phase transition-like events we describe here may represent the most efficient, feasible way for cells to self-organize along a path of least resistance. Intuitively, the straight line is the shortest distance between two points. But in the morpho-space of multi-cellular configurations (Fig. 7), a straight path may not be the shortest path: it may be easier for cells to take a winding route through a landscape of possible tissue architectures. But then, what are the guiding principles that determine this route?

Tissue level morphological phase transitions

Here we look at the phenomenon of multicellular self-organization from the biophysicists' perspective, borrowing the concepts of phase transitions at the tissue level. The term "phase transition" is most commonly used to describe the transformation of matter from one phase/state to another as a function of changes in internal variables or the environment. Phase transitions have recently been shown to mediate cytoplasmic organization at the sub-cellular level. Assembly and disassembly of nucleoli and other nuclear bodies cycles between liquid-phase droplets and solid-phase condensations and can be modulated by rRNA-transcription (35). Phase transition of the microtubule-associated zinc finger protein plays an essential role in the assembly of the spindle apparatus and its associated components (36).

It is compelling to extend this biophysical concept to multicellular self-organization. We consider cells in our assay as particles with certain surface properties, performing a random walk (approximately, see Fig. 2*E*) in a crowded 3D environment. There are two major particle categories, epidermal (E) and dermal (D), so the major inter-particle interactions are E-E, D-D and E-D. Initially epidermal cells form aggregates. When these aggregates reach a certain size, apical-basal polarity develops, leading to the formation of a cyst-like structure. This apical-basal polarity means the inner core and the outer shell of the cyst exhibit different affinities to the environment. Outside of the cyst,

the interaction of basement membrane with dermal fibroblasts and the presence of MMPs destabilizes the cyst structure. The merging of cysts, the fusion of smaller lamellar planes, and thus the eventual large-scale planar configuration, may simply be a straightforward consequence of interactions between cell aggregates whose physical properties are changing over time. The biophysical analogy we draw here, while with a different size scale and dynamics to soft-matter systems, may shed light on how the system self-organizes into different multi-cellular configurations.

Molecular and physical events of organoid formation from newborn skin inspire a strategy to restore hair-formation in adult mice

To profile the molecular events associated with the observed morphological transitions, we analyzed the skin cells' transcriptome. We found that there are four peaks of molecular expression, each corresponding to a tissue phase transition: growth factors for the aggregate formation stage (days 0-2); ECM including collagens for apical-basal polarity and cyst formation (days 1-4); Wnts and MMPs for tissue remodeling in planar formation stage (days 3-6) (Figs. 3-4). Functional perturbation with inhibitors of the key molecules at each phase transition stage can suppress or accelerate the phase transition process (Fig. 5).

The components of these organoid cultures are difficult to dissect. Instead of getting into spatial dissection, we decided to do time point analyses of the whole culture first. This analyses will provide us the first level of information on which molecular pathways are important for the morphological transition between stages. In the future study, we will pursue higher spatial resolution study by sorting epidermal and dermal cells through FACS using endogenous labeling of epidermal (e.g. K14-GFP transgenic mice) and dermal cells (e.g. Pdgfra-EGFP transgenic mice) to do RNA-seq to further differentiate the different molecular pathways involved in the self-organization process. As technology progresses, we will also perform single cell RNA-seq at corresponding time points.

Cells from adult mouse skin are quiescent and normally fail to form hairs. Within the logic of our biophysical analogy, we reasoned that we should be able to restore the phenotype by supplying the

necessary molecules to the adult cells to re-establish phase transition-like self-organization behaviors. We examined the cellular and molecular properties of adult cells to find ways to restore their morphogenetic ability. By mapping the cell configuration back to the morpho-space of Fig. 7, we can appreciate that adult cell cultures are stuck in the aggregation phase (X axis). By RNA-seq, we found that epidermal differentiation genes appear at an early stage. To restore the ability of adult cells to form hair-bearing skin, we designed a protocol based on the new knowledge derived from newborn cell cultures. First, we added inhibitors to PKC to keep cells in undifferentiated states longer. Then we sequentially added three categories of molecules: 1) IGF2 / Vegf; 2) Wnt3a and Wnt10b; 3) MMP14 recombinant proteins at days 0, 1, and 3, respectively, to facilitate progression through the morphogenetic stages. In this way, keratinocyte differentiation is reduced. Thus, under the induction of these sequential added proteins, the morphological transitions are reestablished, and adult cells become competent to reconstitute skin that, upon transplantation, forms hairs robustly.

We identified multiple positive and negative regulatory modules directing the progression of morphological transitions during skin organoid formation (Fig. 5*I*). Instead of focusing on a single molecule, we think it is the successive phase transition-like events that are key to successful self-organization (Fig. 6*D*). More generally, dissociated cells can self-assemble to form many possible multi-cellular configurations (cell aggregates, cysts, tubes, sheets, etc.) in a hypothetical morpho-space (Fig. 7). Between each phases, activators and inhibitors work as a feedback control to stop the earlier phase but initiate the next phase. Thus, simply getting bigger cell aggregates is not useful if they do not progress into cyst stage.

The morpho-space in Fig. 7 can also be useful to appreciate the diverse morphogenetic phenotypes by different epithelial organoids. For example, reconstituted primary mammary myoepithelial cells and luminal cells can form glandular cystic aggregates when placed on Matrigel substrates (2, 37). However, when FGF2 is provided, the cysts undergo branching morphogenesis (38), and do not coalesce toward a planar configuration. In the present study, the end point is a

planar skin with hairs. These results suggest there are molecular specificities among different cell types that steer the transitions through morpho-space to different multi-cellular configurations.

In summary, we propose that the combined use of molecular signals and bio-physical processes may be a basic principle employed by nature to drive morphological transitions from one phase to the next. It is the progression of these phase switches, not specific molecules, that are key to the success of self-organization. By analyzing more examples of organoid morphogenesis in this novel context, we stand to learn more regarding how different physical principles are combined with intrinsic cellular properties to achieve self-organization, thus enhancing our ability to apply these principles to advance tissue engineering.

Materials and Methods

***In vitro* Assay.** As shown in Fig.1*A*, cells were prepared according to our previously described method (19). Usually, the epidermal-dermal ratio is about 1:9 for a piece of back skin in one newborn mouse when we dissociate the back skin into single cells. For the preparation of adult cells, the skins (n≥3) from 2-month-old mice which hair follicles are at refractory telogen phase were peeled off before the hair fibers are plucked through waxing. Then the subcutaneous fat was removed by scissors from the skins, which were then floated onto the 0.25% trypsin solution at 4°C for overnight digestion. The epidermis was scrapped off from the dermis by a scalpel. Then epidermis and dermis were dissociated into single cells as we did for preparing newborn cells. The dissociated epidermal cell and dermal cells were mixed at a ratio of 1:9, and dropped onto to a transwell culture insert that was put in a 6-well culture plate. The lower part of the culture insert was filled with 1.5 ml DMEM/F12 (1: 1, Gibco) culture medium containing 10% FBS (Gibco). The cells were cultured in a humidified atmosphere containing 5 % CO2 at 37°C, with the culture medium being changed every other day.

Live-imaging and Analysis. As shown in SI Appendix, Fig. S2*A*, cells are cultured on a transwell insert that is stuck to a glass culture plate. The plate is covered by a latex membrane to avoid evaporation of the culture medium. The system is kept at 37°C by putting the plate on a heating platform and by heating the lens which is immersed in the culture medium. LSM5 meta confocal microscope was used to film the cellular behaviors. The resulting four-dimensional (3D space plus time) cellular images were then tracked using the commercially available Imaris software at Broad CIRM Center at USC.

Full Methods and any associated references are available in the Supporting Information.

ACKNOWLEDGMENTS. C.-M.C., R.B.W., T.X.J., P.W. are supported by NIH grants AR42177 and AR60306. M.L. is supported by Project funded by China Postdoctoral Science Foundation (2016M590866), Fundamental Research Funds for the Central Universities (106112015CDJRC231206), Special Funding for Postdoctoral Research Projects in Chongqing (Xm2015093), and a fellowship from the China Scholarship Council (2011605042). L.Y. is supported by Innovation and Attracting Talents Program for College and University (‘111’ Project) (B06023), and National Nature Science Foundation of China (11532004, 31270990). W.T.J. is supported by Academia Sinica Research Project on Nanoscience and Technology and Ministry of Science and Technology of Taiwan. L.J.S. was funded by the UK Engineering and Physical Sciences Research Council (EP/F500394/1) through a studentship at the Life Sciences Interface programme of the University of Oxford’s Doctoral Training Centre; We thank Dr. Qing Liu and Dr. Justin Ichida at CIRM Center at USC for supporting the small molecule inhibitors; We thank the University of Southern California (USC) Epigenome Core Facility for conducting Illumina transcriptome sequencing, the University of Southern California's Norris Medical Library Bioinformatics Service for assisting with sequencing data analysis; We thank Prof. Philip Maini (University of Oxford), Dr. Philip Murray (University of Dundee), members of the devBio discussion group at the Wolfson Centre for

Mathematical Biology, Dr. Christoph Weber (MPI PKS, Dresden), Dr. Tian Yang, Dr. Xiaohua Lian (both in the Third Military Medical University), Dr. Chin-Lin Guo (Academia Sinica) and Dr. Maksim V. Plikus (University of California, Irvine) for helpful discussions.

Author Contributions

Designed the research, C.M.C., M. L, R.B.W and L.Y. Performed research and analyses, M.L. Performed the mathematical analysis, L.J.S. and R.E.B. Prepared the RNA-seq libraries, M.L. and P.W. Analyzed RNA-seq data, Y.C.L. and M.L. Designed live-imaging system, C.Y.Y. Performed transplantation assay, T.X.J. Wrote the paper, C.M.C., M.L., R.B.W., L.J.S., W.T.J. and R.E.B.

Author Information The authors declare no competing financial interests. Correspondence and requests for materials should be addressed to C.M.C. (cmchuong@usc.edu).

References

1. Lo AT, Mori H, Mott J, & Bissell MJ (2012) Constructing three-dimensional models to study mammary gland branching morphogenesis and functional differentiation. *J Mammary Gland Biol Neoplasia* 17(2):103-110.
2. Cerchiari AE*, et al.* (2015) A strategy for tissue self-organization that is robust to cellular heterogeneity and plasticity. *Proc Natl Acad Sci U S A* 112(7):2287-2292.
3. Joraku A, Sullivan CA, Yoo J, & Atala A (2007) In-vitro reconstitution of three-dimensional human salivary gland tissue structures. *Differentiation* 75(4):318-324.
4. Sato T & Clevers H (2015) SnapShot: Growing Organoids from Stem Cells. *Cell* 161(7):1700-1700 e1701.
5. Eiraku M*, et al.* (2008) Self-organized formation of polarized cortical tissues from ESCs and its active manipulation by extrinsic signals. *Cell Stem Cell* 3(5):519-532.

6. Eiraku M*, et al.* (2011) Self-organizing optic-cup morphogenesis in three-dimensional culture. *Nature* 472(7341):51-56.
7. Lancaster MA & Knoblich JA (2014) Organogenesis in a dish: modeling development and disease using organoid technologies. *Science* 345(6194):1247125.
8. Sasai Y (2013) Cytosystems dynamics in self-organization of tissue architecture. *Nature* 493(7432):318-326.
9. Chuong CM & Richardson MK (2009) Pattern formation today. *Int J Dev Biol* 53(5-6):653-658.
10. Edelman GM (1989) Topobiology. *Sci Am* 260(5):76-82, 84-76, 88.
11. Newman SA & Bhat R (2008) Dynamical patterning modules: physico-genetic determinants of morphological development and evolution. *Phys Biol* 5(1):015008.
12. Bhat R & Bissell MJ (2014) Of plasticity and specificity: dialectics of the microenvironment and macroenvironment and the organ phenotype. *Wiley Interdiscip Rev Dev Biol* 3(2):147-163.
13. Fuchs E (2009) Finding one's niche in the skin. *Cell Stem Cell* 4(6):499-502.
14. Rompolas P & Greco V (2014) Stem cell dynamics in the hair follicle niche. *Semin Cell Dev Biol* 25-26:34-42.
15. Jiang TX*, et al.* (2004) Integument pattern formation involves genetic and epigenetic controls: feather arrays simulated by digital hormone models. *Int J Dev Biol* 48(2-3):117-135.
16. Lichti U*, et al.* (1993) In vivo regulation of murine hair growth: insights from grafting defined cell populations onto nude mice. *J Invest Dermatol* 101(1 Suppl):124S-129S.
17. Zheng Y*, et al.* (2005) Organogenesis from dissociated cells: generation of mature cycling hair follicles from skin-derived cells. *J Invest Dermatol* 124(5):867-876.
18. Toyoshima KE*, et al.* (2012) Fully functional hair follicle regeneration through the rearrangement of stem cells and their niches. *Nat Commun* 3:784.
19. Lee LF, Jiang TX, Garner W, & Chuong CM (2011) A simplified procedure to reconstitute hair-producing skin. *Tissue Eng Part C Methods* 17(4):391-400.

20. Lei M & Chuong CM (2016) STEM CELLS. Aging, alopecia, and stem cells. *Science* 351(6273):559-560.

21. Weber EL & Chuong CM (2013) Environmental reprogramming and molecular profiling in reconstitution of human hair follicles. *Proc Natl Acad Sci U S A* 110(49):19658-19659.

22. Higgins CA, Chen JC, Cerise JE, Jahoda CA, & Christiano AM (2013) Microenvironmental reprogramming by three-dimensional culture enables dermal papilla cells to induce de novo human hair-follicle growth. *Proc Natl Acad Sci U S A* 110(49):19679-19688.

23. Thangapazham RL*, et al.* (2014) Dissociated human dermal papilla cells induce hair follicle neogenesis in grafted dermal-epidermal composites. *J Invest Dermatol* 134(2):538-540.

24. Chuong CM, Cotsarelis G, & Stenn K (2007) Defining hair follicles in the age of stem cell bioengineering. *J Invest Dermatol* 127(9):2098-2100.

25. Tumbar T*, et al.* (2004) Defining the epithelial stem cell niche in skin. *Science* 303(5656):359-363.

26. Collins CA, Kretzschmar K, & Watt FM (2011) Reprogramming adult dermis to a neonatal state through epidermal activation of beta-catenin. *Development* 138(23):5189-5199.

27. Wu B, Crampton SP, & Hughes CC (2007) Wnt signaling induces matrix metalloproteinase expression and regulates T cell transmigration. *Immunity* 26(2):227-239.

28. Pukrop T*, et al.* (2006) Wnt 5a signaling is critical for macrophage-induced invasion of breast cancer cell lines. *Proc Natl Acad Sci U S A* 103(14):5454-5459.

29. Lei M, Inaba M, & Chuong CM (2016) Vertebrate Embryo: Development of the Skin and Its Appendages. *eLS*.

30. Pastor JC*, et al.* (2016) Proliferative vitreoretinopathy: A new concept of disease pathogenesis and practical consequences. *Prog Retin Eye Res* 51:125-155.

31. Williams SE, Beronja S, Pasolli HA, & Fuchs E (2011) Asymmetric cell divisions promote Notch-dependent epidermal differentiation. *Nature* 470(7334):353-358.

32. Driskell RR*, et al.* (2013) Distinct fibroblast lineages determine dermal architecture in skin development and repair. *Nature* 504(7479):277-281.

33. Lee LF, Jiang TX, Garner W, & Chuong CM (2011) A Simplified Procedure to Reconstitute Hair-Producing Skin. *Tissue Eng Part C-Me* 17(4):391-400.

34. Chuong CM, Cotsarelis G, & Stenn K (2007) Defining hair follicles in the age of stem cell bioengineering. *Journal of Investigative Dermatology* 127(9):2098-2100.

35. Berry J, Weber SC, Vaidya N, Haataja M, & Brangwynne CP (2015) RNA transcription modulates phase transition-driven nuclear body assembly. *Proc Natl Acad Sci U S A* 112(38):E5237-5245.

36. Jiang H*, et al.* (2015) Phase transition of spindle-associated protein regulate spindle apparatus assembly. *Cell* 163(1):108-122.

37. Chanson L*, et al.* (2011) Self-organization is a dynamic and lineage-intrinsic property of mammary epithelial cells. *Proc Natl Acad Sci U S A* 108(8):3264-3269.

38. Ewald AJ, Brenot A, Duong M, Chan BS, & Werb Z (2008) Collective epithelial migration and cell rearrangements drive mammary branching morphogenesis. *Dev Cell* 14(4):570-581.

Figure legends

Fig. 1. Morphological phase transitions from dissociated skin progenitor cells to planar hair bearing skin. We developed a two-step system for hair formation, with an *in vitro* phase that allows us to study the self-organization process. (*A*) Experimental design. (*B*) Immunostaining for K14 shows the stepwise self-organization process of epidermal cells. (*C*) Summary diagram of six stages of *de novo* skin formation. (*D*) Robust hair regeneration after the explant is transplanted on a nude mouse and examined at 20 days later. Hair follicles form with normal structures and can cycle. Epidermal cells are from K14-GFP mice. Cells from adult mice do not regenerate hairs using this system. PCD, Post cultured day. (*E*) Immunostaining for P-cadherin shows adults' cells form only small aggregates in the culture. (*F*) Adult cell assays form very small aggregates at days 1 and 2, while those from newborn

mouse progress. (*G*) Schematic of arrested self-organization process in adult cells. Scale bars=100um unless labeled. *p < 0.05, n>100.

Fig. 2. Time-lapse live-imaging movies of collective cell behavior during self-organization. Visualization of epidermal and dermal cells using K14-GFP or Pdgfra-EGFP transgenic mouse lines, respectively. Movies are shown in the supplement. Exemplary analyses are shown schematically here. (*A*) Aggregate formation. Most cells enter the aggregates but a few of them also enter and leave the aggregates. Scale bar, 100um. (*B*) Two aggregates merge together to form a larger aggregate, and form concentric layers. Scale bar, 100um. (*C*) Three aggregates merge and later one detaches while the other two form a larger stabilized aggregate. (*D*) An epidermal aggregate is surrounded by 2-3 dermal cell layers, which are dynamic, shown by FVB-GFP mouse cells. (*E*) Epidermal cells move with low persistence throughout the experiment, as shown by directional autocorrelation of tracked cells. Black lines show the autocorrelation expected when angles are randomly chosen from the range indicated by the schematics next to the color bar. (*F*) Numerical fit of aggregation model to the change in epidermal cell cluster size distribution for the first 36 hours. (*G*) Cyst-like cavity formation in the center of the aggregate. Cells in the center of the aggregate undergo apoptosis, while other cells leave and join the aggregates. (*H*) Aggregates protrude epidermal cell chains to coalesce together. Not all aggregates merge at the same time. (I) Fused aggregates further coalesce to form a larger epidermal plane. (*J*) Time lapse live-imaging of Pdgfra-EGFP mouse cells show dermal cell behaviors. Scale bars=100um. n≥500.

Fig. 3. RNA-seq profiling and bio-informatics analysis reveal key molecular changes during different times of the self-organization process. RNA-seq data from 0h, 6h, days 1, 2, 4, 7 and 10. (*A*) Functional annotations show pathways and genes that are increased at different time points. Gene ontology shows that cell adhesion, insulin signaling and NOD-like receptor signaling pathway-related genes are differentially expressed at 6h; Vegf signaling, extracellular matrix and basement

membrane-related genes are differentially expressed at day 2; Another group of extracellular matrix genes are differentially expressed at day 4; Toll-like receptor, Nf-kB signaling pathway and lysosome-related genes are differentially expressed at day 7. (*B*) Gene expression changes during the key stages. Genes labeled in red are significantly increased whereas those labeled in blue are significantly decreased at different stages. (*C*) Examples of molecular expression sequence from transcriptome profiling. *Pdgfb* is significantly decreased at 6h. *Prkcb*, *Mmp14* and *Ctsl* are significantly increased at day 2, day 4 and day 7, respectively.

Fig. 4. Spatio-temporal molecular expression pattern during the self-organization process. (*A*) Immunostaining shows E-cadherin is highly expressed at 6h, and decreased in the center of aggregate at day 2. (*B*) Immunostaining shows dynamic changes of collagen IV expression. (*C*) In situ hybridization shows *Mmp14* is expressed at both the basal layer of the aggregate at day1 and in dermal cells adjacent to the aggregate (day 2 - 3) or dermal cells aligned between aggregates (day 4). (*D*) In situ hybridization shows epidermal differentiation gene Lce1d is expressed at the suprabasal layers of aggregates and planar skin. Scale bars=100um. *$p < 0.05$, n=9.

Fig. 5. Functional perturbations at different times elucidate molecules that can accelerate or suppress different phase transition stages. (*A*-B) Aggregates are enlarged or decreased in size when treated with PDGFR or IGF-1R inhibitors, respectively. Cells are immunostained with K14. (*C*-*D*) Apical – basal polarity formation is accelerated or disrupted when treated with Col IV recombinant protein or PKC inhibitor, respectively. P-cadherin immunostaining. (*E*-*F*) Coalescence of the aggregates is accelerated or blocked when treated with Tgfbr1 inhibitor or MMP inhibitor (Prinomastat), respectively. K14 immunostaining and live-imaging. (*G*-*H*) Planarization of the aggregates is accelerated or blocked when treated with NFkB inhibitor or MMP13 inhibitor, respectively. (*I*) Schematic of molecular modules involved in the transitions between different morphological stages.

Positive (in purple) and negative (in blue) regulators work in balance to move the process forward. Scale bars=100um. *p < 0.05, n=9.

Fig. 6. Environmental reprogramming of adult cells to generate hair bearing skin. (*A*) RNA-seq profiling shows major differences between newborn and adult mouse cells. *Igf*, *Vegf* and Wnt related genes that are highlighted at different time points. (*B*) EDC genes (e.g. *Sprr1a* and *Lce3c*) are not highly expressed until day 7 in newborn cultures, but begin to increase at 6h in adult cultures. (*C*) Based on these findings, we designed the optimal environmental reprogramming protocol to deliver key molecules at different stages. See SI Appendix, Fig. S7 for comprehensive data. PKC inhibitors (iPKC) are added throughout to suppress epidermal differentiation. Growth factors IGF2, IGFBP3 and VEGF2 recombinant proteins are added first from days 0 to 2. Wnt3a or Wnt10b are then added daily from days 1 to 4. MMP13, 14 are added from days 3 to 6. Then the cultures are transplanted on nude mice. (*D*) Adults' cells now progress through morphological transition to form cysts and coalesce. (*E*) Adults' cells now form larger aggregates *in vitro*. (*F*) Significantly more hairs are regenerated when treated adult cell cultures are transplanted onto the back of nude mice. Scale bars=100um. *p<0.05, n=9.

Fig. 7. Hypothetical morpho-space showing the many possible multi-cellular configurations that take place during morphogenesis of organoid skin cultures. In this space, each axis represents a major change of cell properties and distinct configuration. The self-organization process from dissociated cells to hairy skin can be viewed as a trajectory. Switch of molecular activities are required to move cell collectives from one phase to the next (represented by blank arrows).

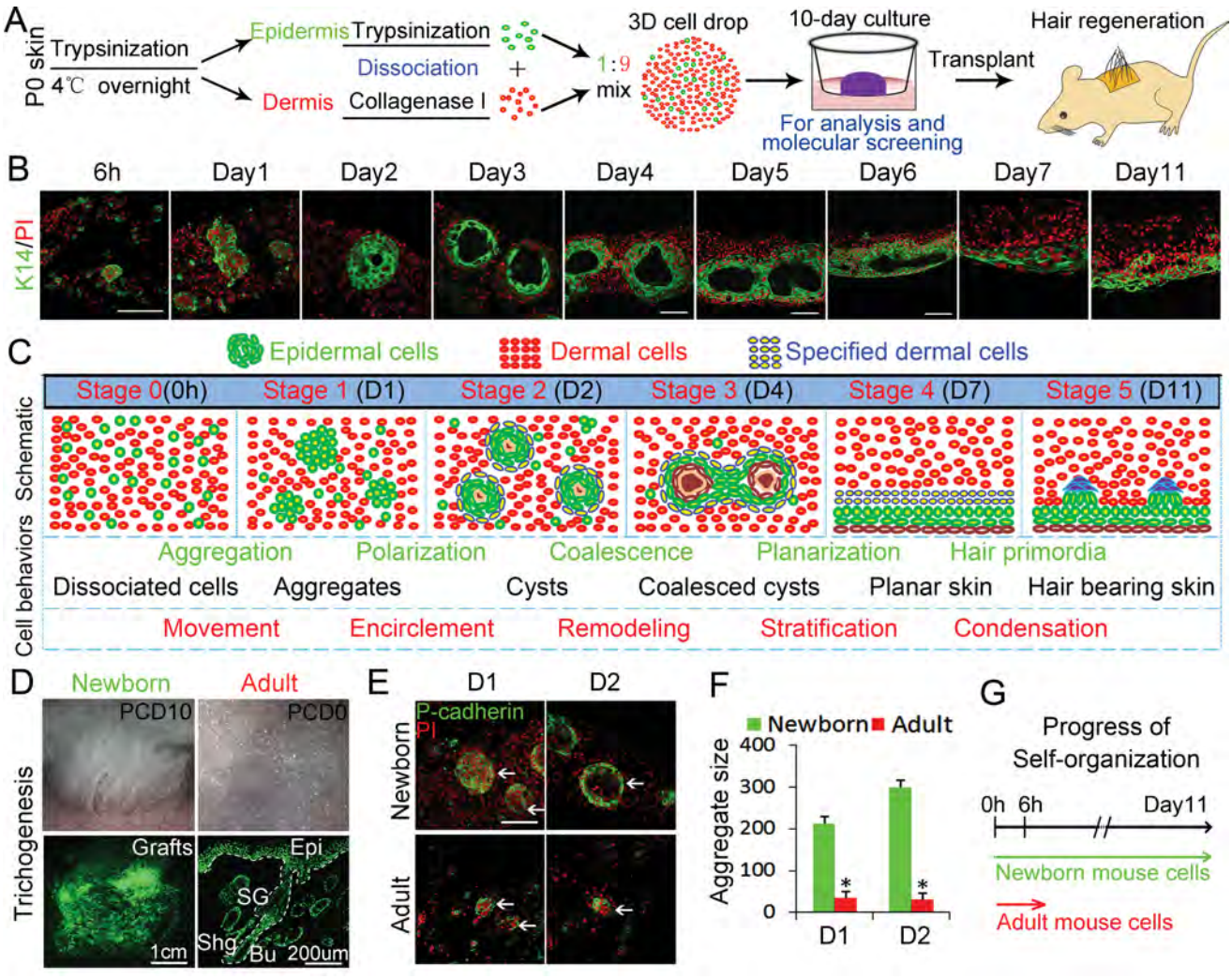
A
P0 skin
Trypsinization
4℃ overnight
Epidermis
Trypsinization
Dissociation
+
Dermis
Collagenase I
1:9
mix
3D cell drop
10-day culture
For analysis and molecular screening
Transplant
Hair regeneration
B
6h
Day1
Day2
Day3
Day4
Day5
Day6
Day7
Day11
K14/PI
C
Epidermal cells
Dermal cells
Specified dermal cells
Stage 0(0h)
Stage 1 (D1)
Stage 2 (D2)
Stage 3 (D4)
Stage 4 (D7)
Stage 5 (D11)
Schematic
Cell behaviors
Aggregation
Polarization
Coalescence
Planarization
Hair primordia
Dissociated cells
Aggregates
Cysts
Coalesced cysts
Planar skin
Hair bearing skin
Movement
Encirclement
Remodeling
Stratification
Condensation
D
Newborn
Adult
PCD10
PCD0
Trichogenesis
Grafts
Epi
SG
Shg
Bu
1cm
200um
E
D1
D2
P-cadherin
PI
Newborn
Adult
F
Newborn
Adult
Aggregate size
400
300
200
100
0
D1
D2
G
Progress of Self-organization
0h
6h
Day11
Newborn mouse cells
Adult mouse cells

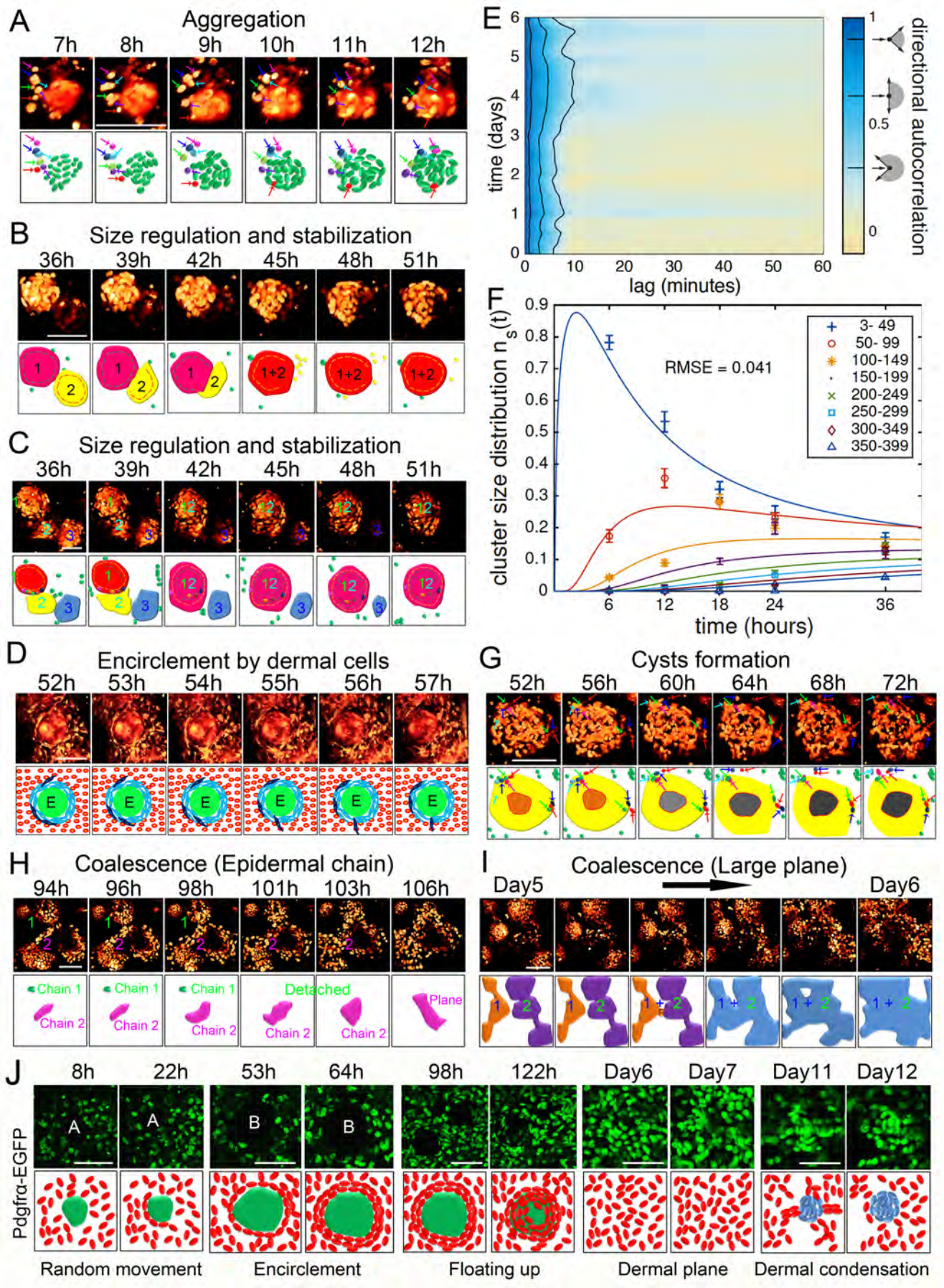
A
Aggregation
7h
8h
9h
10h
11h
12h
B
Size regulation and stabilization
36h
39h
42h
45h
48h
51h
1
2
1+2
C
Size regulation and stabilization
36h
39h
42h
45h
48h
51h
1
2
3
12
D
Encirclement by dermal cells
52h
53h
54h
55h
56h
57h
E
E
Cysts formation
52h
56h
60h
64h
68h
72h
H
Coalescence (Epidermal chain)
94h
96h
98h
101h
103h
106h
1
2
Chain 1
Chain 2
Detached
Plane
I
Coalescence (Large plane)
Day5
Day6
1
2
1 + 2
E
time (days)
lag (minutes)
directional autocorrelation
1
0.5
0
F
cluster size distribution $n_s(t)$
time (hours)
RMSE = 0.041
3- 49
50- 99
100-149
150-199
200-249
250-299
300-349
350-399
J
8h
22h
53h
64h
98h
122h
Day6
Day7
Day11
Day12
A
B
Pdgfrα-EGFP
Random movement
Encirclement
Floating up
Dermal plane
Dermal condensation

A

Functional annotation	Upregulated genes (6h vs 0h)
Cell adhesion	Actg1, Actn1, Cdh1, Csnk2a2, Ctnna1, Egfr, Igf1r, Iqgap1, Lmo7, Met, Nlk, Ptprj, Pvrl2, Vcl
Insulin signaling	Eif4e, Hk1, Hk2, Igf1r, Ikbkb, Map2k1, Nras, Pik3ca, Pik3cb, Prkaa1, Prkar2a, Shc3, Socs3
NOD-like receptor signaling pathway	Birc3, Ccl2, Ccl5, Ccl8, Hsp90aa1, Hsp90ab1, Ikbkb, Il6, Mapk11, Nlrp3, Nod2, Rela, Ripk2
Regulation of actin cytoskeleton	Actg1, Cfl1, Chrm4, Egfr, Ezr, Itga10, Itga5, Itgav, Itgax, Itgb3, Pdgfb, Pik3ca, Pik3cb,

Functional annotation	Upregulated genes (D2 vs D1)
Vegf signaling	Kras, Mapk12, Mapk13, Nos3, Pik3cb,Pla2g2d, Pla2g2f, Pla2g4e, Plcg2, Prkcb, Rac2
Extracellular matrix	Col1a1, Col7a1, Chl1, Fras1, Fmod, Lama1, Lamc2, Mmp2, MMP11, Spon1, Timp3
Basement membrane	Ccdc80, Col7a1, Col8a2, Fras1, Hmcn1, Lama1, Lamc2, Smoc2, Spn, Timp3
Cell-cell junction	Cdh5, Cldn1, Cldn23, Cldn4, Cldn5, Cdsn, Cxadr, Crb3, Dsg1a, Dsg1b, Ocln, Pcdh1

Functional annotation	Upregulated genes (D4 vs D2)
Extracellular matrix	Adamts15, Col18a1, Col8a2, Col6a3, Fbln2, Fgf1, Fn1, Fras1, Frem2, Gpld1, Hpse, Lad1, Lama1, Lamc3, Mamdc2, Mmp12, Mmp14, Mmp17, Ntn4, Spon1, Spon2, Timp2, Timp3, Tgfb1, Tgm2, Wnt10a, Wnt10b, Wnt2b, Wnt9a
Pathways in cancer	Acvr1b, Bcr,Csf1r, Csf2ra, Ccnd1, Cdk6, Dvl3, E2f2, Erbb2, Jun, Fgf1, Fgf3, Fn1, Grb2, Igf1r, Jup, Lamc3, Lama1, Pik3r2, Pik3r5, Cbl, Tgfb1, Wnt10a,Wnt10b, Wnt2b, Wnt9a

Functional annotation	Upregulated genes (D7 vs D4)
Toll-like receptor signaling pathway	Akt1, Cd14, Ccl3, Ccl4, Csnk2a2, Fos, Ikbkb, Irak4, Jun, Mapk11, Mapk13, Mapk3, Map2k1, Map2k3, Map2k4, Myd88, Nfkb1, Nfkb2, Nfkbia, Pik3cb, Pik3r5, Spp1, Ticam1, Ticam2
NF-kB Signaling Pathway	Ikbkb, Map3k1, Map3k7, Myd88, Nfkb1, Nfkbia, Tnfrsf1b, Traf6, Tradd
Lysosome	Abca2, Abcb9, Atp6ap1, Cd68, Ctsb, Ctsc, Ctsd, Ctse, Ctsg, Ctsh, Ctsl, Ctsz, Cltb

B

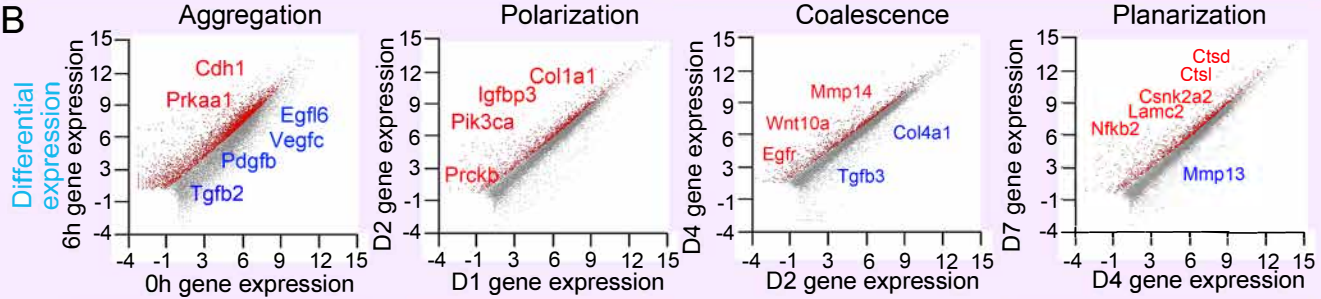

C

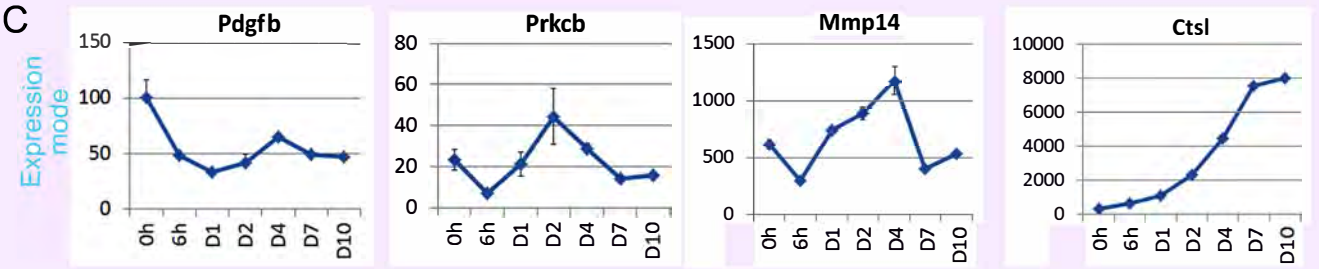

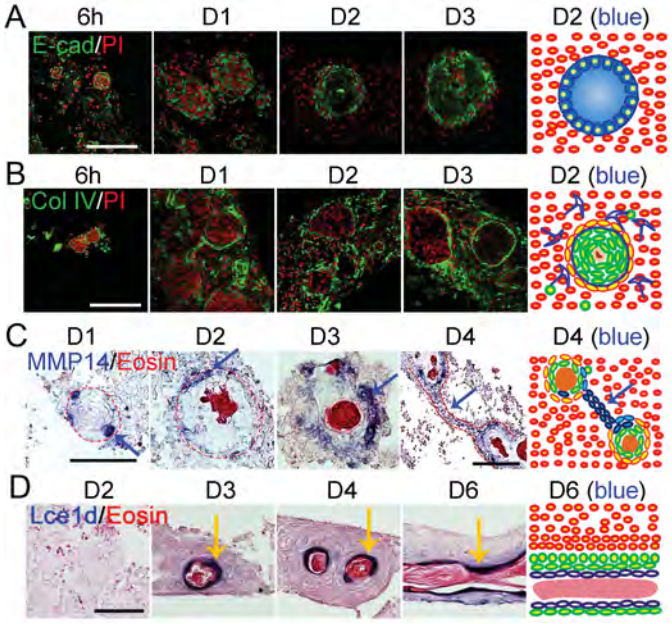
A
6h
D1
D2
D3
D2 (blue)
E-cad/PI
B
6h
D1
D2
D3
D2 (blue)
Col IV/PI
C
D1
D2
D3
D4
D4 (blue)
MMP14/Eosin
D
D2
D3
D4
D6
D6 (blue)
Lce1d/Eosin

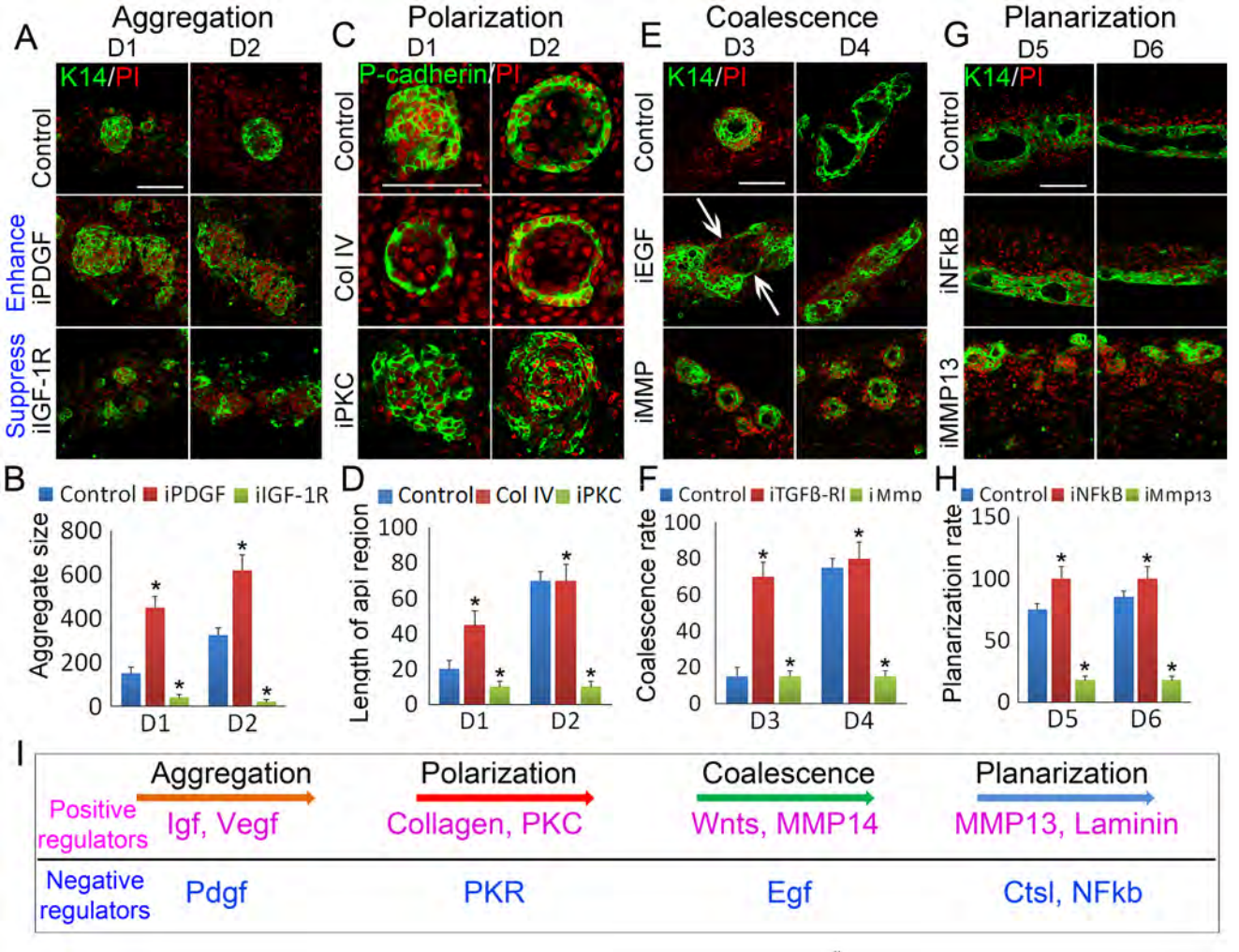
A
Aggregation
D1
D2
K14/PI
Control
Enhance
iPDGF
Suppress
iIGF-1R
C
Polarization
D1
D2
P-cadherin/PI
Control
Col IV
iPKC
E
Coalescence
D3
D4
K14/PI
Control
iEGF
iMMP
G
Planarization
D5
D6
K14/PI
Control
iNFkB
iMMP13
B
Control
iPDGF
iIGF-1R
Aggregate size
800
600
400
200
0
D1
D2
D
Control
Col IV
iPKC
Length of api region
100
80
60
40
20
0
D1
D2
F
Control
iTGFβ-RI
iMmp
Coalescence rate
100
80
60
40
20
0
D3
D4
H
Control
iNFkB
iMmp13
Planarizatioin rate
150
100
50
0
D5
D6
I
Aggregation
Polarization
Coalescence
Planarization
Positive regulators
Igf, Vegf
Collagen, PKC
Wnts, MMP14
MMP13, Laminin
Negative regulators
Pdgf
PKR
Egf
Ctsl, NFkb

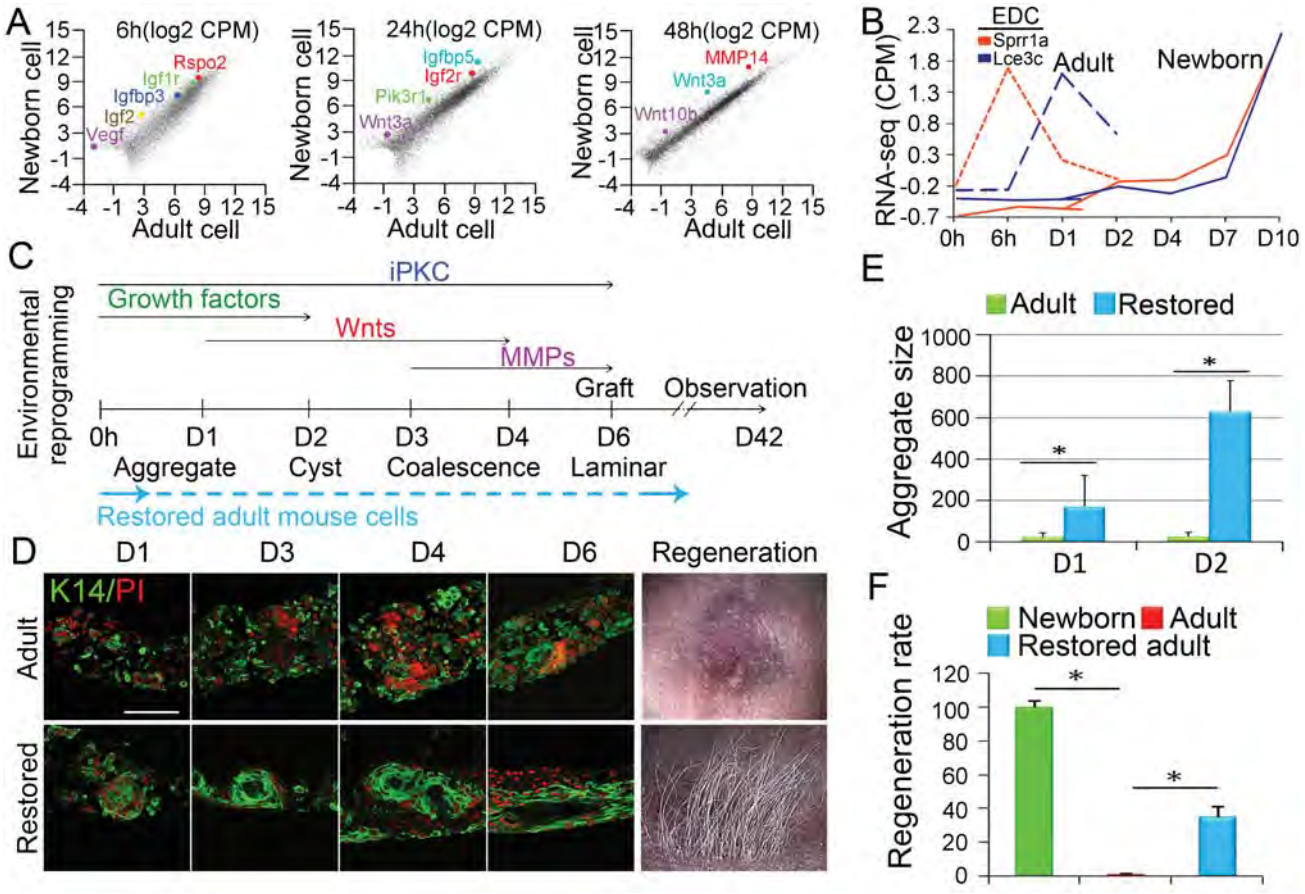
A
6h(log2 CPM)
24h(log2 CPM)
48h(log2 CPM)
Newborn cell
Adult cell
Rspo2
Igf1r
Igfbp3
Igf2
Vegf
Igfbp5
Igf2r
Pik3r1
Wnt3a
MMP14
Wnt3a
Wnt10b
B
EDC
Sprr1a
Lce3c
Adult
Newborn
RNA-seq (CPM)
0h 6h D1 D2 D4 D7 D10
C
Environmental reprogramming
iPKC
Growth factors
Wnts
MMPs
Graft
Observation
0h D1 D2 D3 D4 D6 D42
Aggregate
Cyst
Coalescence
Laminar
Restored adult mouse cells
D
D1 D3 D4 D6 Regeneration
K14/PI
Adult
Restored
E
Adult
Restored
Aggregate size
D1 D2
F
Newborn
Adult
Restored adult
Regeneration rate

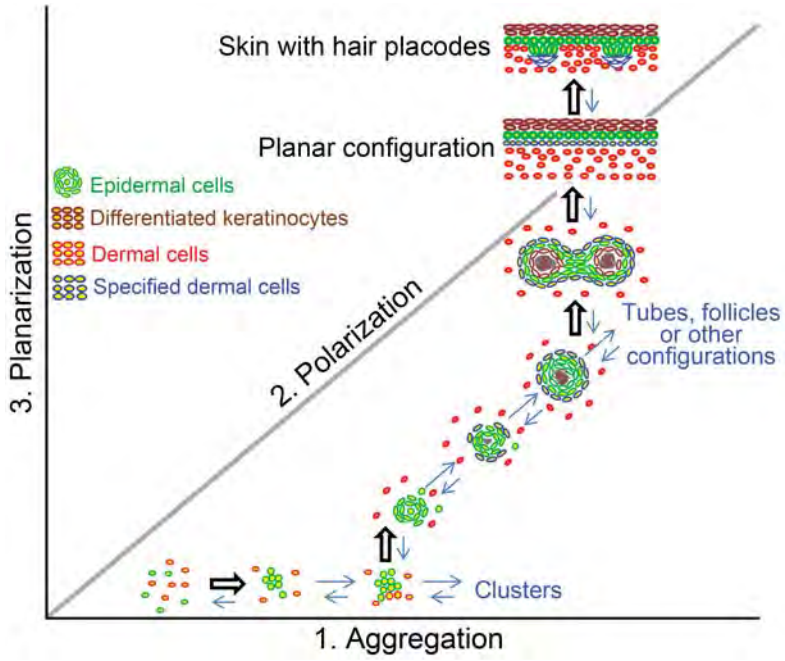
Skin with hair placodes
Planar configuration
Epidermal cells
Differentiated keratinocytes
Dermal cells
Specified dermal cells
2. Polarization
Tubes, follicles
or other
configurations
Clusters
3. Planarization
1. Aggregation